Bull Volcanol (2017) 79: 12
DOI 10.1007/s00445-016-1087-3

RESEARCH ARTICLE

Fragmentation mechanisms associated with explosive lava–water interactions in a lacustrine environment

Erin P. Fitch[1] · **Sarah A. Fagents**[2] · **Thorvaldur Thordarson**[3] · **Christopher W. Hamilton**[4]

Received: 23 May 2016 / Accepted: 27 November 2016 / Published online: 10 January 2017

Abstract Rootless cones form when partially outgassed lava interacts explosively with external water. The explosions represent an end-member system that can elucidate mechanisms of explosive magma–water interactions in the absence of magmatic fragmentation induced by outgassing. The proportion of finely fragmented ejecta (i.e., ash), generated in rootless explosions, may contribute significantly to the energy of the explosion even if the ash volume is small relative to coarser ejecta. Laboratory experiments indicate that the degree of melt–water mixing and energy release are proportional to the abundance of blocky grains, fragmented by brittle disintegration, which effectively contribute thermal energy to the system. To constrain the mechanisms and dynamics of rootless explosive activity, we assess the nature and modes of fragmentation and ejecta characteristics through morphological, textural, and density analysis of rootless tephra associated with a pāhoehoe lava flow in a lacustrine (lake basin) environment. We observe strong correlations between the mean grain size and the mass percentage of both blocky (negative power law trend) and fluidal (positive logarithmic) tephra clasts of all sizes. We interpret these trends as scale-dependent fragmentation behavior due to the decreasing efficacy of hydrodynamic fragmentation as it occurs over finer scales, especially over the ash size range. Additionally, all analyzed beds contain fine ash-sized blocky and mossy clasts, which are thought to be diagnostic of a high transfer rate of thermal to mechanical energy, characteristic of molten fuel–coolant interactions. These results agree with a recent model of rootless cone formation, prior fragmentation theory, and scaled laboratory experiments and therefore provide a field-based analog for future experimental and modeling efforts.

Keywords Rootless cones · Phreatomagmatic · Ash · Molten fuel–coolant interaction · MFCI · Fragmentation

Editorial responsibility: R.J. Brown

Electronic supplementary material The online version of this article (doi:10.1007/s00445-016-1087-3) contains supplementary material, which is available to authorized users.

✉ Erin P. Fitch
epfitch@higp.hawaii.edu

[1] Department of Geology and Geophysics, University of Hawaii, 1680 East-West Road, Honolulu, HI 96822, USA

[2] Hawaii Institute of Geophysics and Planetology, University of Hawaii, Honolulu, HI, USA

[3] Faculty and Institute of Earth Sciences, University of Iceland, Reykjavík, Iceland

[4] Lunar and Planetary Laboratory, University of Arizona, Tucson, AZ, USA

Introduction

In phreatomagmatic eruptions, explosive fragmentation of magma by external water requires an additional transfer of thermal to mechanical energy in the system that is difficult to quantify but can affect the grain size distribution of the resulting tephra (e.g., Houghton and Hackett 1984; Houghton and Schmincke 1986; Morrissey et al. 2000; Zimanowski 2001; Wohletz et al. 2013). Magma–water interactions impart distinguishing grain morphologies that are observable within the resulting deposit (Walker and Croasdale 1971; Heiken 1972, 1974; Heiken and Wohletz 1985) and have been reproduced in laboratory experiments simulating molten fuel–coolant interactions (MFCIs; e.g., Wohletz and McQueen 1981; Wohletz 1983, 1986; Büttner et al. 1999, 2002).

In MFCI theory, fine-grained clasts are associated with rapid conversion of thermal to mechanical energy during the mixing of melt ("fuel") and water ("coolant") and fragmentation subsequent to the collapse of a vapor film between melt and water (e.g., Wohletz 1986; Zimanowski et al. 1997). The energy of the resulting explosion is proportional to the total surface area of the finely fragmented ejecta, termed "active" particles (Büttner and Zimanowski 1998). In contrast, larger "passive" clasts are inferred to form from fragmentation of the envelope of material surrounding the explosion site and do not contribute significant thermal energy to the explosion. Therefore, the proportion of ash generated in a melt–water explosion, even if its volume is relatively small compared to larger ejecta, may represent a significant contribution to the explosion energy release (Zimanowski et al. 2003).

Although laboratory experiments have provided valuable insights, clast morphologies and surface textures observed in MFCI experiments have yet to be compared to the products of their closest natural analog, explosive interactions between subaerial lava flows and water. Rootless explosive activity takes place when largely outgassed lava flows interact explosively with external surface water (Thorarinsson 1951, 1953; Fagents and Thordarson 2007; Belousov et al. 2011), and repeated explosions can build cones of tephra which are termed "rootless cones." Therefore, we investigate the characteristics of rootless tephra to determine the nature and modes of lava fragmentation and thereby constrain the mechanisms and dynamics of explosive activity in rootless eruptions.

Study area

The Rauðhólar rootless cone group is located within the ca. 5200-year-old Elliðaá lava flow of the basaltic Leitin lava flow field (Sinton et al. 2005) southeast of Reykjavík (Fig. 1). Here, tube-fed pāhoehoe passively inundated a lake basin until inflation of the flow caused differential subsidence into water-saturated sediment, fracturing the basal crust and inducing dynamic mixing of molten lava and wet lacustrine sediments, resulting in rootless eruptions (Thordarson and Höskuldsson 2002; Fagents and Thordarson 2007). These rootless eruptions were sustained events as each cone consists of multiple beds. Detailed stratigraphic and grain size analysis was subsequently performed by Hamilton et al. (2017) on one particularly well-exposed cone, "Cone 53," from von Komorowicz (1912).

Hamilton et al. (2017) identified 68 basaltic tephra beds containing lacustrine sediment, which is typically in the form of baked clots. They divided the stratigraphic log of Cone 53 into four units (Fig. 2) and identified alternating fine-grained and coarse-grained paired beds (i.e., bed-pairs). Unit 1 (0–2.01 m) contains nine bed-pairs in addition to six interleaved finer grained beds, containing abundant lacustrine sediment (up to about 60% by mass) and exhibiting low-angle cross-bedding and pinch-and-swell thickness variations. Unit 2 (2.01–7.16 m) contains five bed-pairs that tend to be thicker and coarser grained than the beds in units 1 and 3. Unit 3 (7.16–10.70 m) contains 11 bed-pairs, and unit 4 (10.70–13.55 m) contains three bed-pairs, exhibiting different degrees of welding with the upper members of the bed-pairs being more welded. Beds are named following an A.B.C notation, where *A* is the unit number, *B* is the bed-pair number, and *C* has the value of either 1 or 2 to denote lower or upper bed-pair members, respectively.

Each bed-pair is interpreted by Hamilton et al. (2017) to be the product of an explosion cycle forming first the thinner fine-grained bed followed by the thicker coarse-grained bed. This cycle is inferred to begin with a local recharge of substrate water that fuels the next explosion, resulting in the lower bed-pair layer. The explosion energy declines with time as the flux of external water decreases, resulting in the generation of the upper bed-pair layers, which may have included spray-like jets, lava fountains, or discrete bubble burst events (Mattox and Mangan 1997; Greeley and Fagents 2001), and cessation of activity (i.e., cycle coda) when the water is locally depleted. The interleaved mud-rich layers are interpreted to have been deposited by dilute pyroclastic density currents (PDCs; i.e., surges) and linked with the initiation of new explosion sites within previously undisturbed water-saturated sediment. The combination of (1) decreasing abundance of lacustrine sediment and (2) increasing grain size, with increasing stratigraphic height, is consistent with a reduction in the efficiency of thermal energy transfer from lava to water, thereby decreasing the energy available for fragmentation and dispersal of tephra upon eruption. This change in energetics most likely reflects a reduction in water flux to the explosion center with time (Fagents and Thordarson 2007).

These results help us begin to identify the range of energy regimes during cone formation. The work presented herein builds on that of Hamilton et al. (2017) by investigating the morphologies, textures, and densities of tephra within Cone 53 to further constrain the explosion mechanism based on the fragmentation regimes and ejecta characteristics associated with explosive lava–water interactions.

Fragmentation mechanisms and tephra morphology

The aim of this study is to reconstruct the fragmentation mechanisms acting on the molten lava over a range of

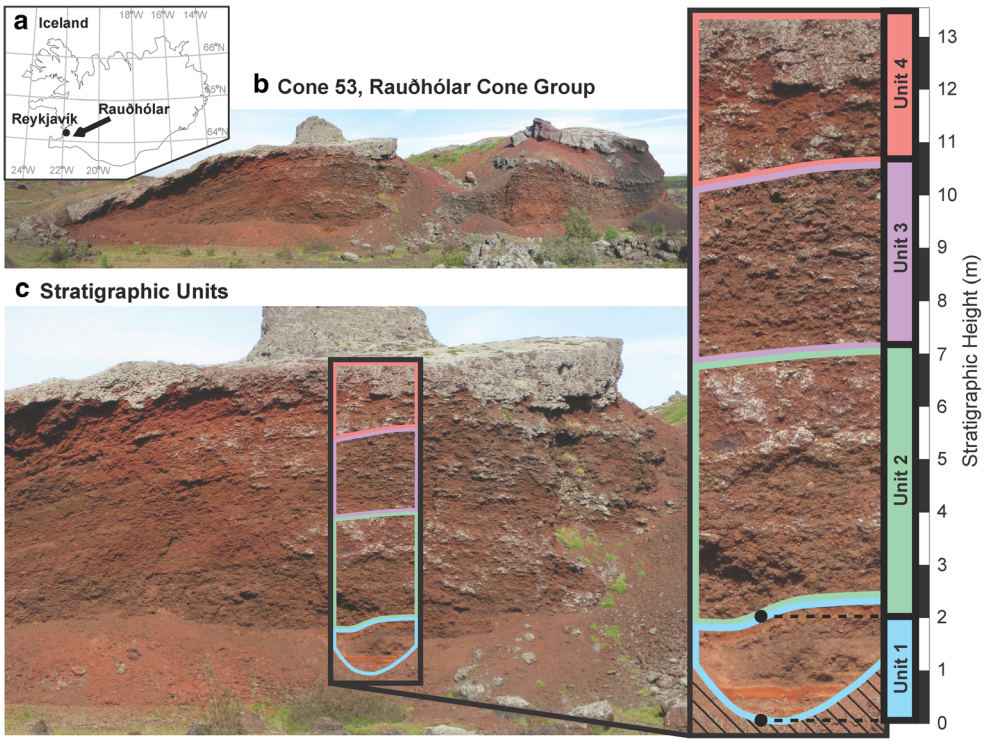

Fig. 1 **a** The location of the Rauðhólar rootless cone group in Iceland, **b** Cone 53 of the Rauðhólar rootless cone group, and **c** the stratigraphic units of Cone 53. The Cone 53 vent location cannot be determined precisely, but the closest exposed crater is located approximately 20 m away from the location of the stratigraphic section (64.095116° N, 21.752074° W)

scales. This is achieved by investigating the morphology of the tephra clasts over a range of sizes (Fig. 3). We therefore draw on theoretical and observational results from the breadth of literature on fragmentation mechanisms relevant to rootless explosions.

In MFCI theory, the finest grains (i.e., referred to as the active particles) are involved in the most efficient and rapid transfer of heat from the molten lava to the water and thought to drive the explosive activity. Therefore, the fragmentation mechanisms acting on a fine scale are tied to the submillimeter-scale dynamics of the melt–water interface. During MFCIs, a vapor film between melt and water can collapse and generate a stress wave that propagates into the melt, resulting in brittle fragmentation if it exceeds the bulk modulus of the melt (termed "stress wave fragmentation" by Wohletz 1983). This stress wave produces *blocky* ash grains dominated by planar to curviplanar surfaces intersecting at nearly right angles (Heiken and Wohletz 1985). Fragmentation of stretched walls in highly expanded bubbles can produce thin, *shard-like* (flake-like or plate-like) ash dominated by curviplanar surfaces. Quench-related or impact-related spallation can also produce shard-like ash grains (Fisher 1968; Morrissey et al. 2000), and the term "limu o Pele" has been used to describe flakes of basaltic glass generated during littoral rootless explosions (e.g., Mattox and Mangan 1997). Hydrodynamic (ductile) disintegration of the melt due to fluid instabilities (Rayleigh–Taylor and Kelvin–Helmholtz) at the interface between melt and a vapor film can result in (1) high-surface-area *mossy* ash grains, when the clast surface cools faster than the timescale of surface tension effects (i.e., the melt behavior is dominated by viscous effects), and (2) *fluidal*, elongate, or drop-like ash (i.e., Pele's hair and Pele's tears, respectively) when surface tension effects dominate melt behavior (Wohletz 1983). *Aggregate* grains are masses of smaller grains that are bonded by mineral precipitates or are tack welded (i.e., agglutinated).

Although the fragmentation energy required to produce ash is larger than that for lapilli or bombs, for an equivalent mass, these larger (passive) clasts still require fragmentation energy and contribute heat to the expanding gas envelope. The morphology of lapilli and bombs depends on both the available fragmentation energy, which is proportional to the energy released by the explosion, and the rheology of the lava flow, which ranges from solid to fluid over the flow profile.

Since the processes driving different fragmentation mechanisms vary over a range of scales, it is important to consider the effect of scale on fragmentation, independent of MFCI processes. Zimanowski et al. (2003) examined this topic with a theoretical and experimental study and found that while brittle fragmentation produced grains of all sizes through a steady increase in strain, hydrodynamic fragmentation requires an exponential increase of three orders of magnitude in fragmentation energy as grain size decreases from coarse to extremely fine ash. In other words, the production of blocky

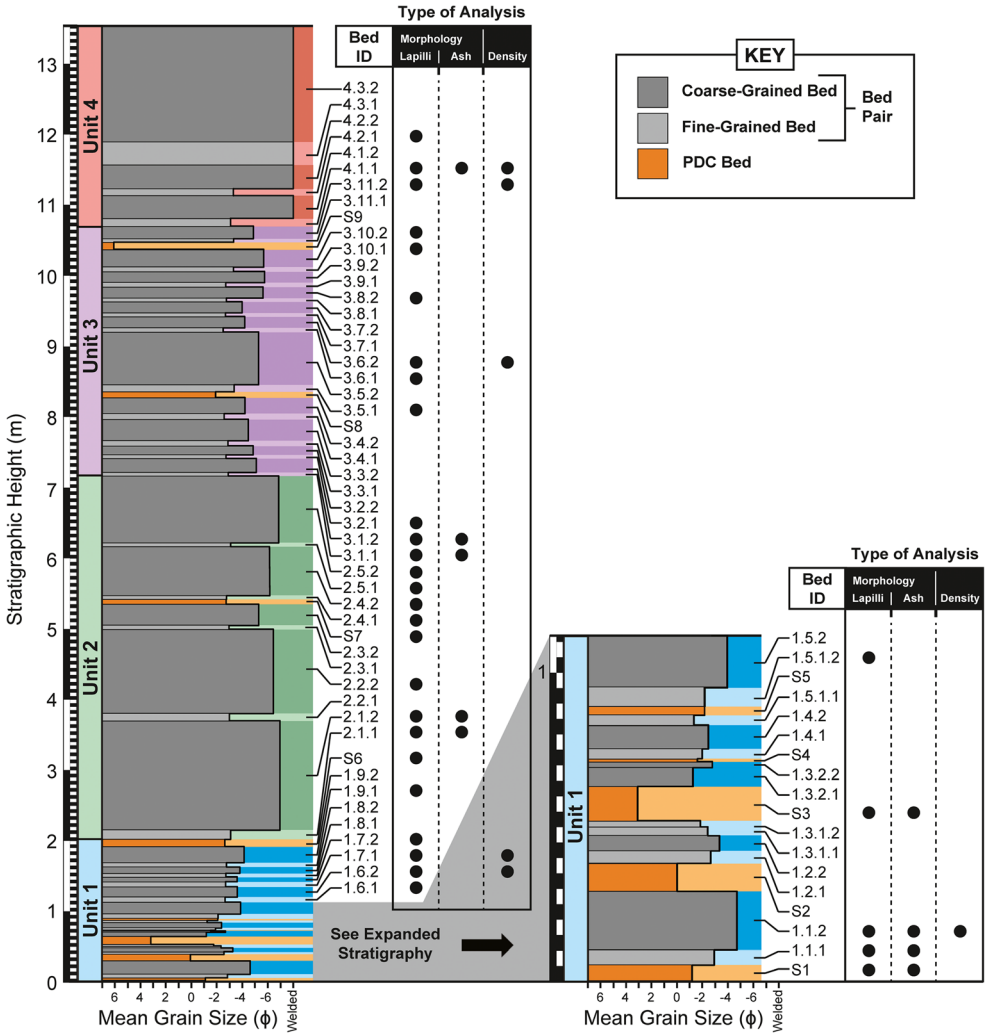

Fig. 2 Stratigraphic log of Rauðhólar Cone 53 showing alternating finer grained beds (*light gray*) and coarser grained beds (*dark gray*) of bed-pairs over four units, with interleaved fine-grained, lacustrine sediment-rich beds (i.e., PDC beds) in *orange*. The samples that underwent morphology (lapilli and ash) and density analysis are indicated by *black circles* in the charts to the right of the stratigraphic logs, in order to show their distribution over the stratigraphy

ash (by brittle fragmentation) becomes energetically more favorable than the production of fluidal ash (by hydrodynamic fragmentation) as grain size decreases. Therefore, we hypothesize that the ash fraction of rootless ejecta will be dominated by blocky grains, but the energy necessary to produce blocky ash in the first place may still require an explosion mechanism like MFCI.

Methods

Ash morphology

To determine the ash-scale fragmentation mechanisms in rootless eruptions, we examined grain morphology over a range of ash sizes. To examine differences or similarities in clast morphology over the four stratigraphic units, as well as differences between bed types (PDC and fine-grained and coarse-grained beds of bed-pairs) within each unit, nine beds were investigated. This includes two PDC beds from unit 1 (beds S1 and S3), the first bed-pairs from units 1, 2, and 3 (beds 1.1.1, 1.1.2, 2.2.1, 2.1.2, 3.1.1, and 3.1.2), and the lowest bed in unit 4 (bed 4.1.1). For each bed, 100 juvenile grains were examined from three size bins: 0.5–0 ϕ (1.41–1.00 mm, very coarse ash), 1.5–2 ϕ (0.354–0.250 mm, medium ash), and 3.5–4 ϕ (88–62 μm, very fine ash). These size bins enabled us to investigate key changes in morphology with decreasing grain size, including the very fine ash grade, which is the inferred size range of active particles in MFCI experiments (Büttner and Zimanowski 1998). Ash grains were classified, following the scheme of Heiken and Wohletz (1985), in accordance with their dominant morphology as blocky, fluidal, mossy, shard-like, or aggregate, as is summarized in Fig. 3.

Lapilli morphology

Lapilli-sized and bomb-sized rootless ejecta are inferred to be part of the passive clasts formed from fragmentation of

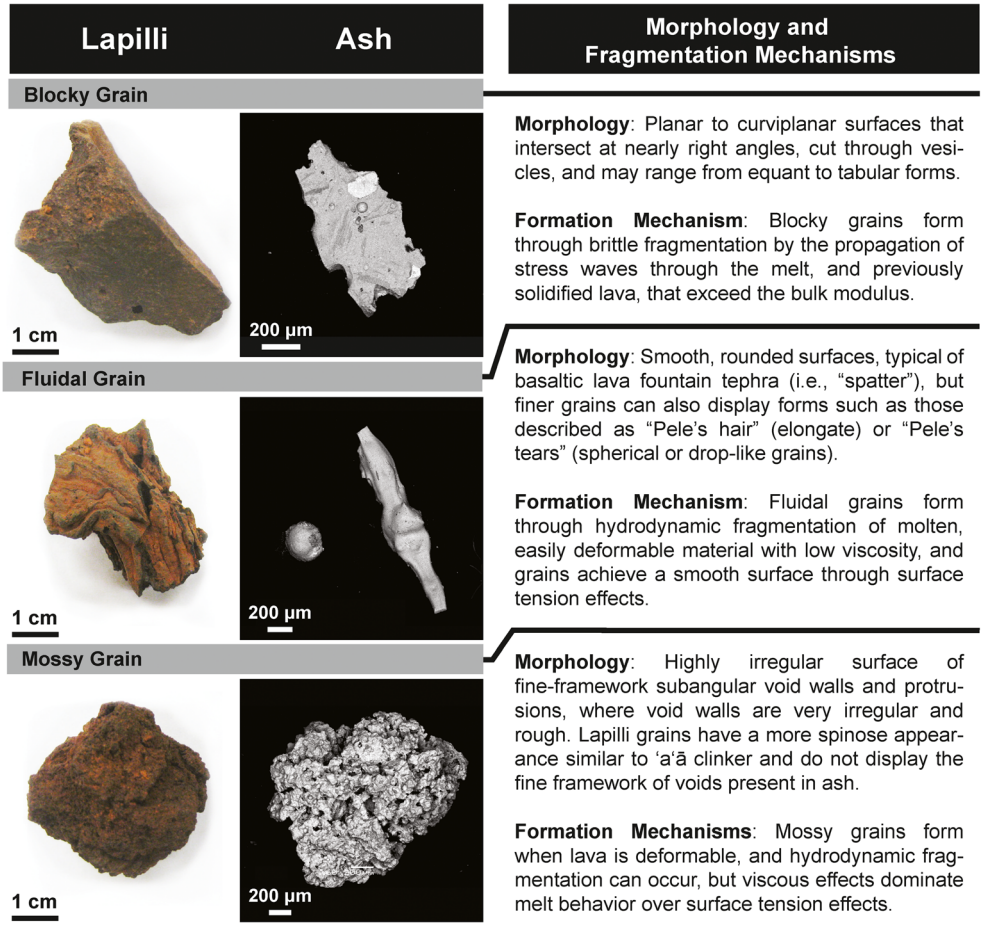

Fig. 3 Blocky, fluidal, and mossy morphologies associated with rootless lapilli and ash. Ash grains are shown in backscatter electron images

the envelope of material surrounding the explosion site. To assess the fragmentation mechanisms producing passive clasts, coarse lapilli were analyzed because this is the coarsest material present in the majority of the deposits and is also the size range typically used for measuring vesicularity (Houghton and Wilson 1989, see "Lapilli vesicularity and component analysis" section). We analyzed lapilli from 31 beds, including unit 1 beds (total = 11 beds; three bed-pairs, three PDC beds, and two other beds), unit 2 beds (total = 8 beds; three bed-pairs, one PDC bed, and one other bed), unit 3 beds (total = 10 beds; three bed-pairs and four other beds), and unit 4 beds (total = 2 beds), which include the beds involved in ash analysis. For all beds, except S1 and S3, at least 100 coarse lapilli clasts from the size class between −4 and −5 ϕ (16–32 mm) were classified according to the dominant morphology as "blocky," "mossy," or "fluidal" (Fig. 3). However, for S1 (n = 12) and S3 (n = 50), medium lapilli clasts between −3 and −4 ϕ (8–16 mm) were examined since coarse lapilli were rare or absent. The proportions of each morphology making up the surface of individual lapilli grains were also estimated. For example, a grain dominated by fluidal morphology, but with 20% of its surface made up of fractured surfaces and 10% of its surface morphology made up of a spinose, irregular morphology, would be described as 70% fluidal, 20% blocky, and 10% mossy.

Surface textures and lacustrine sediment

Ash adhered to tephra surfaces is common for phreatomagmatic and rootless tephra (e.g., Heiken and Wohletz 1985; Mattox and Mangan 1997) and is considered evidence for a lower energy "wet" eruption or explosion, where water is abundant in the ejecta envelope and can act as an adhering agent prior to cementation by mineral precipitates (Morrissey et al. 2000). However, tack welding of ash on the surface of melt fragments prior to quenching may also take place if low-energy explosions produce very fluidal ejecta. Additionally, rapid cooling and contraction of the outer surface of still-molten tephra that comes into contact with water may form quench cracks depending on the amount of water in the ejecta envelope (Büttner et al. 1999, 2002). Therefore, we documented these features using a scanning electron microscope (SEM) and optical microscope (cf., Zimanowski et al. 1997; Büttner et al. 1999, 2002).

The characteristics of lacustrine sediment contained within the rootless tephra provide information on the

pre-explosion sediment–melt mixing as well as interfacial instabilities and subsequent fragmentation during lava–sediment interaction. Building on the observations of Hamilton et al. (2017), we recorded the abundance of lapilli with significant coatings of sediment and the occurrence of lacustrine sediment within juvenile ejecta, during lapilli morphology analysis ("Lapilli morphology" section).

Lapilli vesicularity and component analysis

To obtain a robust, unbiased baseline of rootless tephra vesicularity, we measured the density of 606 lapilli clasts from samples of six randomly chosen beds from the samples that underwent morphology analysis, using standard methods outlined in Houghton and Wilson (1989). A preliminary test of waterproof coating methods reviewed in Houghton and Wilson (1989), for 100 grains, revealed that wax coating gives density values 9% (σ = 3%) lower than spray coating, on average, which is higher than the 1% or less found by Houghton and Wilson (1989). Since we observe that much more volume is gained using wax coating than is lost using spray coating, we chose spray coating for Rauðhólar grains to reduce the average error. We converted density to vesicularity, using a dense rock equivalent (DRE) value of 2860 kg m^{-3}, since this value was the highest measured density. This value is higher than the estimated DRE using standard calculations (Gualda et al. 2012) and an average Leitin lava composition of 48% SiO_2, 2% TiO_2, 15% Al_2O_3, 12% FeO, 9% MgO, 12% CaO, and 2% Na_2O from Sinton et al. (2005). Additionally, since viscosity and vesicularity change over different parts of the lava flow profile, we investigated the source material of rootless tephra from within the parent lava flow, using (a) measured vesicularity, (b) qualitative observations of vesicle size and spatial distribution, and (c) clast morphology data to classify the tephra components, and compared our observations with field observations of tube-fed pāhoehoe lava.

Statistical correlation

To determine potential relationships between physical processes associated with rootless tephra formation, we calculated correlation (r) and determination (r^2) coefficients between datasets. To identify significant correlations, we conservatively interpret determination coefficient values from 0 to 0.30 as a negligible correlation, 0.31–0.50 as a weak correlation, 0.51–0.70 as a moderate correlation, and 0.71–1.00 as a strong correlation. Therefore, we interpret a correlation as strong if more than 70% of the variance in the dataset can be accounted for by the model.

Results

Ash morphology

We found that the rootless ash size fraction is primarily composed of blocky, mossy, and fluidal grains, glassy shards, and a minor component (≤2%) of aggregates of smaller pyroclasts (Table 1). Typically, the proportions are as follows: (1) The very coarse ash fraction contains blocky (9–58%), mossy (8–36%), and fluidal (28–67%) grains only; (2) the medium ash fraction contains blocky (32–76%), mossy (9–39%), and fluidal (15–43%) grains with a minor abundance of glassy shards (≤8%); and (3) the very fine ash fraction is dominated by blocky grains (53–80%), with lower shard (12–34%) and fluidal (4–24%) components. The percentage of fluidal grains decreases with decreasing grain size, and the percentage of blocky grains increases with decreasing grain size (Fig. 4). Based on compositional analysis using an energy-dispersive spectroscope (EDS), we found that free crystals make up <1% of the ash fraction, so the increase in blocky grains is not related to an increasing free crystal component. Peaks in mossy ash grain abundance occur exclusively between very coarse and medium ash, and shards only begin to appear in fine ash.

A series of paired-sample t tests were conducted to determine whether there are significant differences in the means of blocky, fluidal, and mossy abundances (in %) over the coarse, medium, and fine ash analysis size ranges (significance level α = 0.05; degrees of freedom = 8). We did not find a significant difference in the means of coarse and medium mossy ash ($p = 5 \times 10^{-1}$), but all other sample pairs displayed a significant difference in the means: (a) coarse and fine blocky ($p = 3 \times 10^{-4}$), fluidal ($p = 3 \times 10^{-5}$), and mossy ash ($p = 2 \times 10^{-4}$); (b) coarse and medium blocky ($p = 2 \times 10^{-3}$) and fluidal ash ($p = 1 \times 10^{-3}$); and (c) medium and fine blocky ($p = 2 \times 10^{-2}$), fluidal ($p = 1 \times 10^{-4}$), and mossy ash ($p = 4 \times 10^{-4}$). These results suggest that the patterns observed for fluidal and blocky ash, with decreasing grain size, are significant. Furthermore, we observe a strong positive linear correlation (r = 0.84, r^2 = 0.71) between mean grain size and fluidal ash abundance, indicating that hydrodynamic fragmentation is more prevalent among the coarser ash fractions. Although a weak negative linear correlation (r = −0.64, r^2 = 0.41) is observed between mean grain size and blocky ash abundance, a moderate negative linear correlation (r = −0.81, r^2 = 0.65) is present between blocky and fluidal ash-grade clast abundance, indicating that brittle fragmentation occurs at the expense of hydrodynamic fragmentation.

Table 1 Ash morphology analysis results

Bin size	Bed	Blocky	Fluidal	Mossy	Shard	Aggregate
−0.5 to 0 ϕ (1.41–1.00 mm, very coarse ash)	S1	31	43	26	0	0
	S3	57	35	8	0	0
	1.1.1	43	28	29	0	0
	1.1.2	34	30	36	0	0
	2.1.1	26	58	16	0	0
	2.1.2	18	68	14	0	0
	3.1.1	30	40	30	0	0
	3.1.2	9	56	35	0	0
	4.1.1	33	33	34	0	0
Mean ± Standard Deviation		31 ± 14	43 ± 14	25 ± 10	0	0
1.5 to 2 ϕ (0.354–0.250 mm, medium ash)	S1	49	30	16	4	1
	S3	61	23	12	4	0
	1.1.1	59	27	12	2	0
	1.1.2	45	24	26	5	0
	2.1.1	39	27	26	8	0
	2.1.2	32	43	23	2	0
	3.1.1	39	22	39	0	0
	3.1.2	41	21	38	0	0
	4.1.1	76	15	9	0	0
Mean ± Standard Deviation		49 ± 14	26 ± 8	22 ± 11	3 ± 3	1 ± 0
3.5 to 4 ϕ (88–62 μm, very fine ash)	S1	59	5	0	34	2
	S3	71	4	0	24	1
	1.1.1	65	10	1	22	2
	1.1.2	64	9	0	26	1
	2.1.1	53	15	4	28	0
	2.1.2	55	24	5	16	0
	3.1.1	69	7	1	23	0
	3.1.2	80	6	1	12	1
	4.1.1	59	14	0	27	0
Mean ± st. dev.		64 ± 9	10 ± 6	1 ± 2	24 ± 7	1 ± 1

Fluidal ash characteristics

Elongate fluidal grains are present in beds S3 (i.e., the medium ash fraction) and 4.1.1 (i.e., the very fine ash fraction), but they are more consistently present in the medium to very fine ash fraction of the unit 2 beds (1–4%). Botryoidal grains, made up of unbroken vesicles with smooth surfaces, make up 2% of coarse and medium ash fractions in bed S1, but <1% of all other beds. A very minor proportion (<5%) of drop-like grains is present in the very fine ash fraction of all beds examined except bed 1.1.1, which did not contain any drop-like grains. Formation of drop-like grains that are <200 μm in diameter requires, according to theory, very high interfacial accelerations (Zimanowski et al. 2003), although Wohletz and McQueen (1984) suggest that a metal oxide melt could form grains smaller than 100 μm, due to lower surface tension of the metal alloy. However, we analyzed five drop-like, two blocky, and two other fluidal grains in the size range of 88–62 μm with EDS, taking at least three shot points per grain, and found that all have similar basaltic glass compositions, with an average composition (notated as average ± standard deviation) of 50 ± 2% SiO_2, 2 ± 0% TiO_2, 13 ± 2% Al_2O_3, 11 ± 2% FeO, 7 ± 1% MgO, 11 ± 1% CaO, and 4 ± 1% Na_2O.

Blocky ash mass percentages

We estimated the mass percentage of juvenile ash consisting of blocky grains (hereafter referred to as *blocky ash mass percent*) for each bed analyzed, by multiplying the average abundance of blocky grains (i.e., the number of blocky grains in 100 grains, averaged over the three size bins analyzed) by the mass percent of juvenile ash. We found that PDC beds have three to four times the blocky ash mass percent of finer grained beds of the bed-pairs, which have two to eight times that of coarser

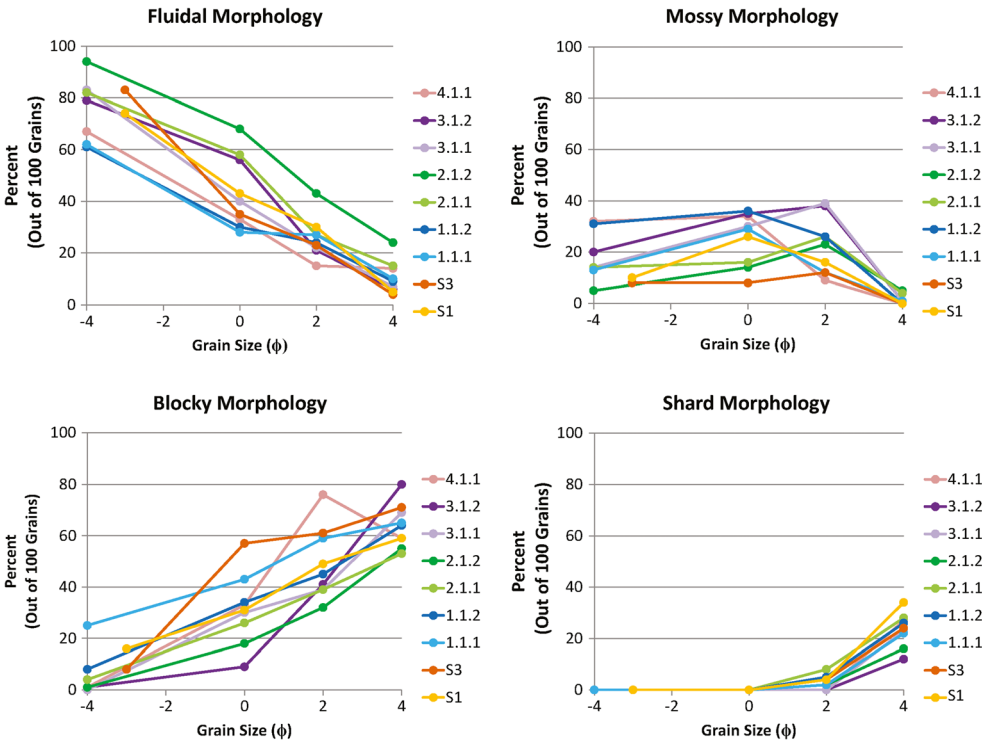

Fig. 4 Graphical depiction of ash and lapilli morphology analysis results for fluidal, mossy, blocky, and shard abundances. The ash bins analyzed, −0.5–0 ϕ (1.41–1.00 mm, very coarse ash), 1.5–2 ϕ (0.354–0.250 mm, medium ash), and 3.5–4 ϕ (88–62 μm, very fine ash), are stylized as 0, 2, and 4 ϕ along the horizontal axis. The lapilli morphology analysis for the bed-pairs, between −4 and −5 ϕ (16–32 mm, coarse lapilli), and for the PDC beds, between −2 and −3 ϕ (4–18 mm, medium lapilli), is also displayed for context

grained beds (Fig. 5a). This is generalized by a strong negative power law correlation ($r = -0.98$, $r^2 = 0.96$) between mean grain size and blocky ash mass percent of each bed, which follows the inherent negative power law relationship between mean grain size and ash mass percent ($r = -0.96$, $r^2 = 0.92$) (Fig. 5b). In comparison, fluidal and mossy ash mass percentages show, respectively, strong ($r = -0.89$, $r^2 = 0.79$) and moderate ($r = -0.79$, $r^2 = 0.62$) negative power law relationships with mean grain size.

Lapilli morphology

We found that lapilli-sized clasts are dominated by fluidal morphology (61–94%) with lower abundances of mossy (5–32%) and blocky (1–25%) clasts (Figs. 4 and 6). Unit 1 displays the widest range of clasts consisting of more than one morphology type, with a significantly larger abundance of dominantly blocky clasts than the other units, based on *t* tests assuming unequal variances, and using data displayed in Fig. 6a (significance level $\alpha = 0.05$; $p = 1 \times 10^{-2}$ for both unit 2 and unit 3 against unit 1). Units 2 and 3 display a tighter clustering of points near the fluidal vertex, and unit 3 is almost exclusively composed of dominantly fluidal and mossy clasts (Fig. 6). These trends indicate a progressive shift from a broader range of morphologies to a more tightly clustered, fluidal distribution of morphologies over units 1–3. Unit 4, being dominated by thick, welded beds, also follows this trend. Despite unit-scale trends, there are no consistent differences >10% in the average abundance of each lapilli morphology type (fluidal, mossy, blocky) among the three bed types (PDC and fine-grained and coarse-grained beds of bed-pairs) (Table 2). Additionally, negligible correlations are observed between mean grain size and blocky, mossy, and fluidal lapilli abundances. Furthermore, no consistent

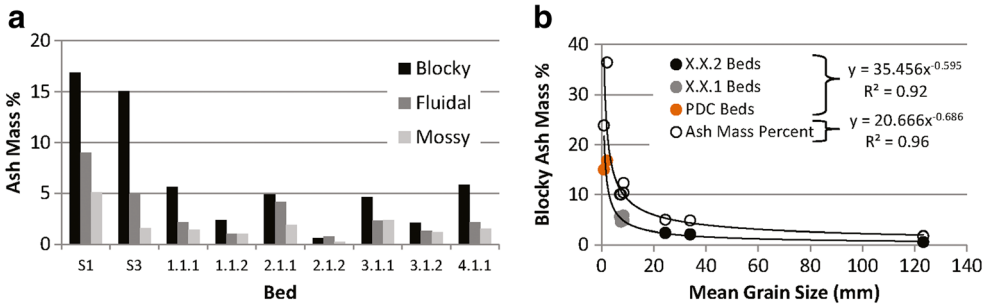

Fig. 5 **a** Histogram of blocky, fluidal, and mossy ash mass percent results and **b** mean grain size plotted against blocky ash mass percent and total ash mass percent, with power law trendlines

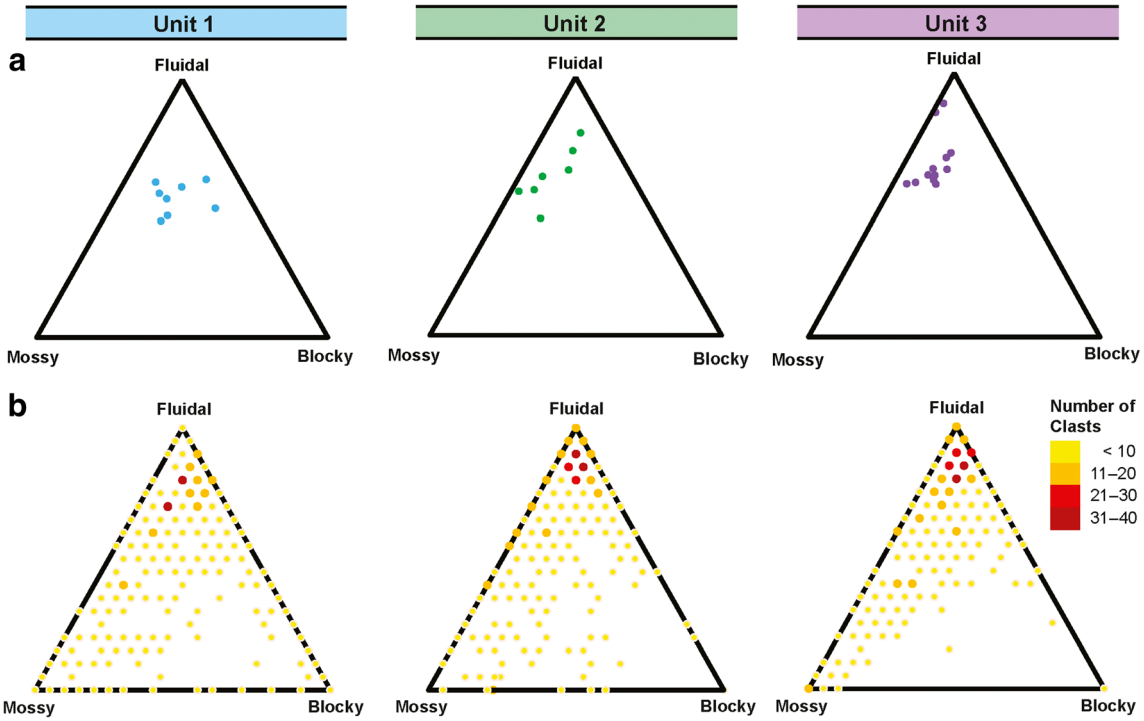

Fig. 6 **a** Ternary diagrams of the total lapilli morphology averages for each bed analyzed within each unit (25 beds, 25 data points). Average fluidal, mossy, and blocky percentages were taken over all clasts within the sample set for each bed, based on the dominant morphology of each clast. **b** Ternary diagrams, one for each unit, displaying the complete combined data for three bed-pairs in each unit (six beds total), with points "color weighted," based on the number of clasts displaying the same characteristics, i.e., *darker colors* represent larger numbers of clasts occupying a given location on the ternary diagram, in order to highlight overall trends

patterns in the distribution of individual clast morphologies within each bed are present among the three bed types (Online Resource 1).

Total fluidal and blocky clast mass percents

Fluidal grains dominate grain sizes larger than coarse ash; therefore, we estimated the mass percent of ejecta that underwent hydrodynamic fragmentation (hereafter referred to as *total fluidal clast mass percent*), across all grain sizes. For bomb-sized ejecta, based on field observations, we estimate that all ejecta larger than −6 ϕ (64 mm) are >90% fluidal clasts by mass. For medium to coarse lapilli (−6 and −2 ϕ; 64–8 mm), we used the results from "Lapilli morphology" section, and for clasts smaller than −2 ϕ (4 mm), we used the results from "Ash morphology" section. We then calculated the fluidal mass percent as in "Blocky ash mass percentages" section for beds S1, S3, 1.1.1, 1.1.2, 2.1.1, 2.1.2, 3.1.1, 3.1.2, and 4.1.1. We found a strong, positive logarithmic correlation between mean grain size and total fluidal clast mass percent ($r = 0.95$, $r^2 = 0.90$) (Fig. 7a), which is stronger ($\Delta r^2 = 0.11$) than the power-law correlation between mean grain size and

Table 2 Lapilli morphology analysis results

Bed-pair layer	Blocky (%)	Fluidal (%)	Mossy (%)	Number of beds
Unit 4.X.2	N/A (welded)	N/A (welded)	N/A (welded)	N/A (welded)
Unit 4.X.1	1 ± 0	66 ± 2	34 ± 2	2
Unit 3.X.2	2 ± 2	80 ± 6	18 ± 6	5
Unit 3.X.1	2 ± 2	75 ± 7	22 ± 7	5
Unit 2.X.2	5 ± 5	74 ± 20	20 ± 15	4
Unit 2.X.1	2 ± 2	76 ± 5	22 ± 7	3
Unit 2.X.1	7 ± 4	72 ± 12	21 ± 14	3
Unit 1.X.1	10 ± 9	67 ± 12	23 ± 11	5
PDC beds	9 ± 5	63 ± 20	27 ± 24	4

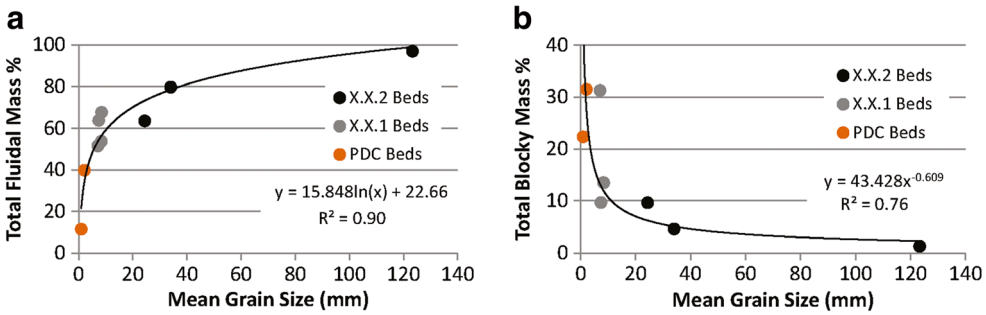

Fig. 7 **a** Mean grain size plotted against total fluidal clast mass percent, with logarithmic trendline, and **b** mean grain size plotted against total blocky clast mass percent, with power law trendline

ash-grade fluidal clast abundance. Therefore, the former correlation provides a better constraint on the relationship between hydrodynamic fragmentation and explosion energy.

We calculated the total blocky clast mass percent as above. However, blocky clasts larger than −6 ϕ (64 mm) are rare and therefore have a negligible effect on the total estimate. We found a strong, negative power law correlation between mean grain size and total blocky clast mass percent (r = −0.87, r^2 = 0.76) (Fig. 7b), but it is much weaker (Δr^2 = 0.20) than that observed between mean grain size and blocky ash mass percent.

Surface textures and lacustrine sediment

Adhered juvenile ash grains are commonly found on rootless tephra, although present in highly variable abundances. They are typically associated with fluidal surfaces, which display minor surface deformation at the contact between the ash and the pyroclast surface. This suggests that juvenile ash grains are largely tack-welded to partially molten tephra surfaces prior to surface quenching. Localized polygonal cracks are observed on clasts from all beds examined (Fig. 8), but not on ash grains, in contrast to the quenched ash produced in MFCI experiments (e.g., Büttner et al. 1999, 2002). Polygonal cracks on lapilli clasts are not likely associated with the expansion of volatiles (bread crusting), because they are localized and present on both vesicular and very dense fluidal clasts. We found negligible correlations between the abundance of clasts with localized polygonal cracks and lacustrine sediment mass percent or mean grain size, suggesting that they form independent of explosion energy. Hamilton et al. (2017) observe that polygonal cracks are typically found on the underside of clasts and interpreted that they result from enhanced cooling on the bottom of the clasts that occurs due to interactions with water (or steam) in the post-depositional environment.

All pyroclasts show some degree of lacustrine sediment coating (i.e., mineral grains and diatom fragments), confirmed through SEM and EDS analysis, which gives the beds an overall red-orange appearance (Fig. 8). The millimeter-scale contact between a thick, hard sediment coating and the pyroclast surface is irregular, and void size within the sediment decreases away from the interface (Fig. 9). Therefore, the sediment may have been partly fused, cooling around expanding gas trapped in the sediment. Small (<1 mm) fragments of dark glass are embedded in the sediment, possibly due to quench spallation of the tephra surface and subsequent transport of spalled grains into the sediment as water at the interface vaporized. Additionally, hardened aggregates of lacustrine sediment, ranging in grain size from fine ash to coarse lapilli, are found in all deposits. They contain up to 10–25% blocky ash fragments and are also commonly embedded in the tephra (Fig. 8). Where lacustrine sediment is confined within the submillimeter folds of a fluidal grain (Fig. 10), these folds are surrounded by vesicles along the boundary between sediment and the melt surface. Blocky and shard-like ash-sized fragments from the melt surface appear to have been incorporated into the lacustrine sediment within the fold. The vesicles may be vaporized water from within the pore space of the lacustrine sediment, and the non-explosive growth of these vesicles may have been preceded by fluid instabilities.

Lapilli vesicularity and component analysis

Lapilli clast density (a total of 606 clasts measured from six beds) ranged from 1000 to 2900 kg m^{-3} (0–70% vesicularity) and displayed a unimodal distribution with an overall mean of 1500 kg m^{-3} (51% vesicularity) and standard deviation of 300 kg m^{-3} (11% vesicularity) (Fig. 11). The mean density of clasts from individual beds ranged from 1300 to 1600 kg m^{-3} (54–39% vesicularity) with standard deviations ranging from 200 to 300 kg m^{-3} (7–10% vesicularity).

Based on the lapilli clast morphology of 31 beds (3071 clasts total) and vesicularity measurements of six beds (606 clasts total), we identified four types of clasts, described in Fig. 12, types A, B, C, and D, in relation to their source location from within the parent lava flow. We infer that types A, B, and C are *lava lithics*, derived from the upper lava crust, and make up approximately 1% of the ejecta by volume and have a mean vesicularity of 14 ± 9% (11 clasts), with a maximum of 28%. Type A is likely sourced from the outer crust, where rapid cooling trapped bubbles at an early stage of growth, producing homogeneously sized and dispersed bubbles (27 ± 1% mean vesicularity; three clasts). Type B is likely derived from the mid-crust, where heat from the lava tube, and

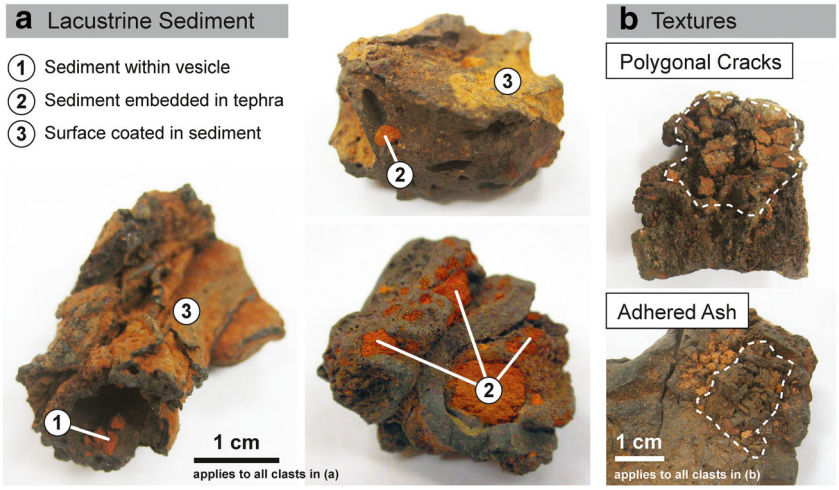

Fig. 8 (a) Evidence of lava and lacustrine sediment intermingling is clearly observable in these lapilli from beds 1.1.2, 1.7.2, and 2.1.1. Sediment may be embedded within the tephra, affixed inside of vesicles, or coat the outer surface of clasts. Note also the prevalence of uncoated fracture surfaces, for comparison (b) Textural characteristics of pyroclast surfaces include shallow polygonal cracks and adhered ash.

insulation from the outer crust, enabled bubbles to grow and potentially coalesce before solidification (16% vesicularity; only one clast measured). Type C is likely derived from the dense inner crust prior to solidification, where bubbles can migrate out into the mid-crust, but a viscosity difference impedes the travel of bubbles from the lava tube to the inner crust (8 ± 3% mean vesicularity; seven clasts). Type D is derived from the molten material within the lava tube, producing fluidal or mossy surfaces and heterogeneously sized bubbles (51 ± 10% mean vesicularity; 594 clasts). Fluidal type D clasts with very low vesicularities (<20%) make up <1% of the ejecta by volume and may have been sourced from material located near the basal crust, where lava could have remained hot, but gas bubbles would have moved up and out of the basal layer due to buoyancy and shearing. Some percentage of ejecta is likely to have fallen back into the vent and subsequently been recycled and re-expelled from the explosion site (Houghton and Wilson 1989; Houghton and Smith 1993). Although armored (i.e., cored) clasts are common among the bomb-sized population, based on field observations made by Hamilton et al. (2017), we did not find any obvious armored lapilli during morphology analysis. However, we found that approximately 3% (by volume) of lapilli are notably rounded with abraded surfaces, which provides a minimum estimate of the percentage of recycled lapilli.

Discussion

Scale-dependent characteristics of explosion ejecta

We observed strong correlations between mean grain size and blocky ash mass percent (negative power law), total blocky clast mass percent (negative power law), and total fluidal clast mass percent (positive logarithmic) for the nine beds examined in detail (Figs. 5b and 7). This implies that at lower fragmentation energies (larger mean grain sizes), an increase in fragmentation energy results in a small increase in the percentage of blocky clasts and small decrease in the percentage of fluidal clasts. Conversely, at high fragmentation energies (smaller mean grain sizes), a small increase in fragmentation energy results in a substantial increase in the percentage of

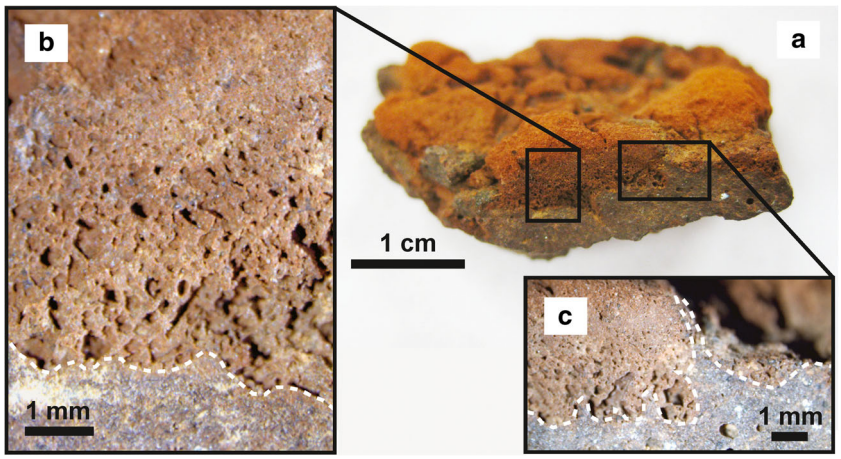

Fig. 9 The contact between lava and lacustrine sediment is clearly observable in this lapillus from bed 1.1.1. This contact appears sharp in **a**, but under an optical microscope, in **b** and **c**, the contact is irregular, with lava and sediment interfingering over a region typically smaller than 1 mm (marked by *white dashed line*). Additionally, in **b** and **c**, voids are clearly present in the sediment and begin to decrease in size away from the interface over a 1 to 2-mm length

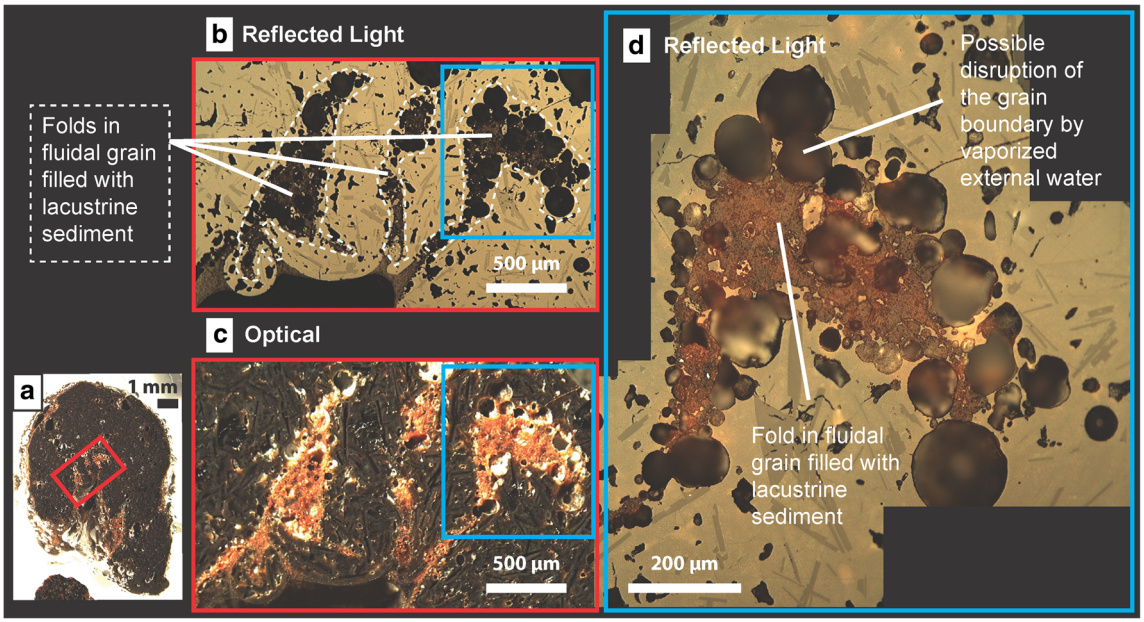

Fig. 10 Lacustrine sediment is confined within the submillimeter folds of a fluidal grain, shown in **a**. In **b**, the folds are shown in a reflected light image obtained with a petrographic microscope and are outlined with a white *dashed line*. In **c**, orange lacustrine sediment is clearly visible in this optical image of the same area as in **b**, obtained with a binocular microscope. In **d**, a further magnified reflected light image displays a fold surrounded by vesicles along the boundary between sediment and the melt surface. Blocky and shard-like ash-sized fragments are also visible within the lacustrine sediment filling the fold

blocky clasts (particularly ash) and significant decrease in the percentage of fluidal clasts. This trend is consistent with scale-dependent fragmentation behavior predicted by Zimanowski et al. (2003), as outlined in "Fragmentation mechanisms and tephra morphology" section. Therefore, the observations that (1) coarser grained beds contain more fluidal clasts and a lower percentage of blocky clasts (particularly in the ash fraction) than the finer grained beds of the bed-pairs and (2) PDC beds contain fewer fluidal clasts and a larger percentage of blocky ash grains than both members of the bed-pairs are consistent with scale-dependent fragmentation mechanisms and the assertion that mean grain size is proportional to the explosion energy. These trends are relevant for juvenile tephra only, as juvenile mean grain size was calculated for samples with >10% mass percent lacustrine sediment, and furthermore, the calculation of fluidal and blocky ash mass percent utilized only juvenile material.

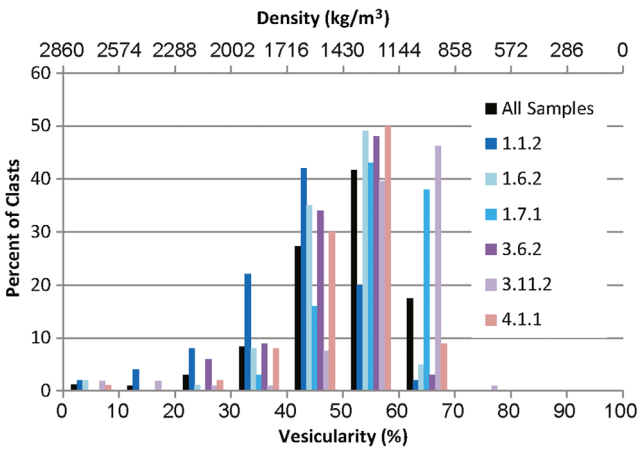

Fig. 11 Vesicularity histograms of the six beds analyzed (606 clasts total)

Modeling and laboratory experiments predict that fluidal ash grains smaller than 100–200 μm are unlikely to be produced, because they require high interfacial accelerations (Zimanowski et al. 2003). However, rootless ash contains fluidal grains as small as 88–62 μm, with a transition from fluidal-dominated to blocky-dominated ash between 1410 and 88 μm. Given that no compositional differences were detected that could affect melt surface tension, such as the presence of higher metal oxide abundance, as suggested by Wohletz and McQueen (1984), these pyroclasts were likely sourced from lava that had undergone minimal cooling.

Implications for the explosion mechanism of rootless cones

Detailed analysis of rootless ejecta has revealed evidence of dynamic interactions between lava and water–saturated sediment during rootless eruptions. The presence of lacustrine sediment within tephra (Figs. 8 and 10) indicates a dynamic mixing environment that was vigorous enough to allow water and sediment to be incorporated into lava, confining water in a way similar to the setup of MFCI experiments. Sediment

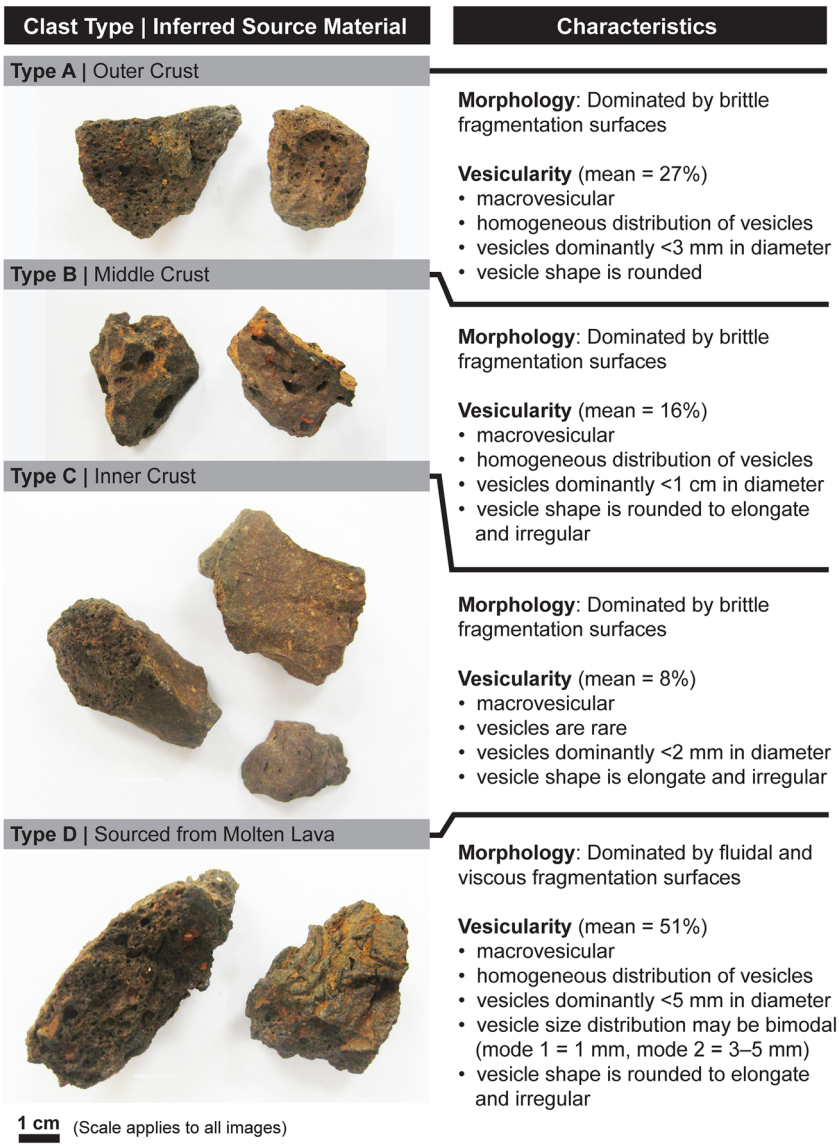

Fig. 12 Clast material source classifications

adhered to the surface of tephra, and between the layers of armored bombs (Hamilton et al. 2017), demonstrates that abundant lacustrine sediment was present in the ejecta envelope. The presence of water-related quench cracks on rootless tephra, in addition to the fact that some lacustrine sediment-rich PDC beds contain bomb sags, suggests that the ejecta envelope must have contained liquid water or condensing vapor during some explosions. Lastly, the presence of ash, and especially fine ash, in all beds indicates that some portion of the ejecta formed under conditions of high heat transfer, which requires dynamic mixing of lava and water.

The mass percent of ash in rootless beds displays a strong negative power law relationship with mean grain size (Fig. 5b), in agreement with MFCI experiments, which have shown that explosion energy correlates negatively with mean grain size (e.g., Wohletz and McQueen 1984). The energetic significance of the fluidal, mossy, and blocky ash morphologies recorded can also be assessed through MFCI theory. Wohletz (1983) asserts that blocky ash forms through stress wave fragmentation and drop-like and mossy ash form through fluid instability fragmentation (as outlined in "Fragmentation mechanisms and tephra morphology" section), and since these morphologies are observed in rootless ash, the triggering of lava–water explosions may involve both mechanisms. Initial fluid instability fragmentation at the melt–water mixing interface may have formed fluidal and mossy ash, and as heat transfer increased via enhanced melt disintegration, the sequential disruption caused by multiple collapses of the vapor film may have initiated stress waves large enough to overcome the bulk modulus of the melt (i.e., producing

"detonation" waves). This could have resulted in a shift to brittle fragmentation, producing blocky ash grains and triggering an MFCI feedback loop of heat transfer and further fine fragmentation.

According to this model, the fine blocky ash grains are the main thermodynamic driver of the explosions, even though mossy and drop-like morphologies may have been formed prior to the generation of detonation waves. Blocky grains dominate very fine ash 62–88 μm (3.5–4 ϕ). Other workers also observe that blocky ash grains associated with MFCI experiments (i.e., active particles) are typically smaller than 3 ϕ (125 μm; Heiken and Wohletz 1985; Wohletz 1986; Büttner et al. 1999, 2002), and grains interpreted to be active particles have also been observed in phreatomagmatic ash smaller than 3 ϕ (Dellino et al. 1990; Dellino and La Volpe 1995; Büttner et al. 1999, 2002; Dellino et al. 2001). Therefore, the presence of fine to extremely fine blocky ash in rootless ejecta is consistent with previously studied products of natural and experimental explosive melt–water interactions.

After initiation of an explosive MFCI, during vapor expansion, fragmentation of the overlying lava column produces coarser tephra with a range of morphologies, dependent on lava rheology and fragmentation energy, and subsequent ejection of tephra from the explosion site occurs. Although fluidal and mossy tephra dominates the ejecta, the presence of lava lithics as well confirms that all parts of the parent lava are ejected during a rootless explosion. Drop-like ash may have also been produced during this stage, as suggested by Zimanowski et al. (1997, 2001), as well as elongate fluidal ash (Pele's hair), as observed during littoral rootless explosions (Mattox and Mangan 1997) and MFCI experiments (Wohletz and McQueen 1984; Zimanowski et al. 1997; Büttner et al. 2002). Finally, secondary breakage and abrasion of ejecta through recycling may have contributed to the production of blocky or rounded ejecta or armored clasts if the recycled clasts fall into a pocket of molten lava in the vent before being re-ejected in an explosion.

The shards observed in the medium–fine ash fraction of all beds are likely to have been produced by quench-related or impact-related spallation and (or) the fragmentation of botryoidal ash. Botryoidal ash and bubble-wall shards may form concurrently to drop-like grains at the melt–water mixing interface or may have formed during ballistic transport of ejecta in free air. These seemingly fragile grains are likely preserved because of their resistance to fragmentation from thermal quenching (e.g., Patel et al. 2013).

Vesicularity of rootless tephra

Rootless lapilli at Rauðhólar range in vesicularity from 0 to 70% and are dominated by fluidal and mossy clasts with a mean vesicularity of 51%, compared with 14% (28% maximum) for lava lithics. The mean vesicularity of rootless tephra at the pāhoehoe-fed Ice Harbor cone field in Idaho, measured by Reynolds et al. (2015), is 23%, which does not include lava lithics. This range of vesicularities is comparable to the span of vesicularities observed in pāhoehoe lavas (e.g., Wilmoth and Walker 1993; Cashman et al. 1994; Gaonac'h et al. 1996; Herd and Pinkerton 1997; Robert et al. 2014). Basaltic tephra from magmatic lava fountaining events, by comparison, typically have an average vesicularity greater than 50% and a maximum vesicularity greater than 70% (e.g., Mangan and Cashman 1996; Polacci et al. 2009; Stovall et al. 2011, 2012). Although processes such as shock-induced decompression (Carey et al. 2012) or ingestion of external water by lava (Edwards et al. 2013) may increase vesicularity in rootless tephra, the analyses required to quantify the effect of these processes are beyond the scope of this work.

Conclusions

We conclude that rootless eruptions at Rauðhólar are likely driven by processes similar to MFCI experiments, which are associated with a high transfer rate of thermal to mechanical energy, resulting in the generation of blocky and mossy ash. Explosion ejecta of all sizes display scale-dependent fragmentation behavior, and therefore, the tephra morphology of coarse-grained and fine-grained beds of bed-pairs, as well as PDC beds, is largely dependent on explosion energy. These findings are consistent with the model presented by Hamilton et al. (2017) where bed-pairs form through a two-stage process involving a higher energy opening phase (forming the fine-grained bed) followed by a lower energy phase (forming the coarse-grained bed), continuing until water availability diminishes. PDC beds represent even more energetic explosions, based on the finer grain size of juvenile ash and larger abundance of lacustrine sediment, and decrease in number with time as the rootless cone is constructed.

The identification of processes similar to MFCIs as the driving mechanism for lacustrine rootless eruptions associated with a tube-fed pāhoehoe flow, based on tephra analysis, is a testament to the value of fragmentation theory and scaled laboratory experiments. In the same way that our understanding of a natural system has benefited from theoretical and experimental pursuits, our hope is that this work informs future experiments and models, in order to better constrain the energetics of natural analogs of MFCIs.

Acknowledgements We would like to thank the Icelandic Institute of Natural History for generous access to the study area. We are grateful to Gary Huss, Ryan Ogliore, Aurelien Thomen, Elizabeth Koeman, and

Myriam Telus at the Hawai'i Institute of Geophysics and Planetology for help with sample preparation and assistance with SEM and EDS analysis. We also thank Bruce Houghton, Scott Rowland, John Sinton, Maria Janebo, and Samantha Isgett at the University of Hawai'i Department of Geology and Geophysics for helpful discussions. This work was supported by NSF EAR-1119648 HIGP publication number 2240 and SOEST publication number 9876.

References

Belousov A, Behncke B, Belousova M (2011) Generation of pyroclastic flows by explosive interaction of lava flows with ice/water-saturated substrate. J Volcanol Geotherm Res 202(1):60–72

Büttner R, Dellino P, La Volpe L, Lorenz V, Zimanowski B (2002) Thermohydraulic explosions in phreatomagmatic eruptions as evidenced by the comparison between pyroclasts and products from molten fuel coolant interaction experiments. J Geophys Res: Solid Earth 107(B11):ECV 5-1–ECV 5-14

Büttner R, Dellino P, Zimanowski B (1999) Identifying magma-water interaction from the surface features of ash particles. Nature 401(6754):688–690

Büttner R, Zimanowski B (1998) Physics of thermohydraulic explosions. Phys Rev E 57(5):5726–5729

Carey RJ, Manga M, Degruyter W, Swanson D, Houghton B, Orr T, Patrick M (2012) Externally triggered renewed bubble nucleation in basaltic magma: the 12 October 2008 eruption at Halema'uma'u overlook vent, Kīlauea, Hawai'i, USA. J Geophys Res: Solid Earth 117(B11202)

Cashman KV, Mangan MT, Newman S (1994) Surface degassing and modifications to vesicle size distributions in active basalt flows. J Volcanol Geotherm Res 61(1):45–68

Dellino P, Frazzetta G, La Volpe L (1990) Wet surge deposits at La Fossa di Vulcano: depositional and eruptive mechanisms. J Volcanol Geotherm Res 43(1):215–233

Dellino P, Isaia R, La Volpe L, Orsi G (2001) Statistical analysis of textural data from complex pyroclastic sequences: implications for fragmentation processes of the Agnano-Monte spina tephra (4.1 ka), Phlegraean fields, southern Italy. Bull Volcanol 63(7): 443–461

Dellino P, La Volpe L (1995) Fragmentation versus transportation mechanisms in the pyroclastic sequence of Monte Pilato-Rocche Rosse (Lipari, Italy). J Volcanol Geotherm Res 64(3–4):211–231

Edwards BR, Karson J, Wysocki R, Lev E, Bindeman I, Kueppers U (2013) Insights on lava–ice/snow interactions from large-scale basaltic melt experiments. Geology 41(8):851–854

Fagents SA, Thordarson T (2007) Rootless volcanic cones in Iceland and on Mars. In: Chapman MG (ed) The geology of Mars: evidence from earth-based analog. Cambridge University Press, United Kingdom, pp. 151–177

Fisher RV (1968) Puu Hou littoral cones, Hawaii. Geol Rundsch 57(3): 837–864

Gaonac'h H, Stix J, Lovejoy S (1996) Scaling effects on vesicle shape, size and heterogeneity of lavas from Mount Etna. J Volcanol Geotherm Res 74(1):131–153

Greeley R, Fagents SA (2001) Icelandic pseudocraters as analogs to some volcanic cones on Mars. J Geophys Res: Planets 106(E9):20527–20546

Gualda GA, Ghiorso MS, Lemons RV, Carley TL (2012) Rhyolite-MELTS: a modified calibration of MELTS optimized for silica-rich, fluid-bearing magmatic systems. J Petrol 53(5):875–890

Hamilton CW, Fitch EF, Fagents SA, Thordarson T (2017) Rootless tephra stratigraphy and emplacement processes. Bull Volcanol doi:10.1007/s00445-016-1086-4

Heiken G (1972) Morphology and petrography of volcanic ashes. Geol Soc Am Bull 83(7):1961–1988

Heiken G (1974) An atlas of volcanic ash. Smithsonian Institution Press, Washington, DC

Heiken G, Wohletz K (1985) Volcanic ash. University Press, California, Chicago, Harvard & MIT

Herd RA, Pinkerton H (1997) Bubble coalescence in basaltic lava: its impact on the evolution of bubble populations. J Volcanol Geotherm Res 75(1–2):137–157

Houghton B, Hackett W (1984) Strombolian and phreatomagmatic deposits of Ohakune craters, Ruapehu, New Zealand: a complex interaction between external water and rising basaltic magma. J Volcanol Geotherm Res 21(3):207–231

Houghton B, Schmincke H (1986) Mixed deposits of simultaneous strombolian and phreatomagmatic volcanism: Rothenberg volcano, east Eifel volcanic field. J Volcanol Geotherm Res 30(1): 117–130

Houghton B, Smith R (1993) Recycling of magmatic clasts during explosive eruptions: estimating the true juvenile content of phreatomagmatic volcanic deposits. Bull Volcanol 55(6):414–420

Houghton B, Wilson C (1989) A vesicularity index for pyroclastic deposits. Bull Volcanol 51(6):451–462

Mangan MT, Cashman KV (1996) The structure of basaltic scoria and reticulite and inferences for vesiculation, foam formation, and fragmentation in lava fountains. J Volcanol Geotherm Res 73(1):1–18

Mattox TN, Mangan MT (1997) Littoral hydrovolcanic explosions: a case study of lava–seawater interaction at Kilauea volcano. J Volcanol Geotherm Res 75(1–2):1–17

Morrissey M, Zimanowski B, Wohletz K, Buettner R (2000) Phreatomagmatic fragmentation. In: Houghton B, Rymer H, Stix J, McNutt S (eds) Encyclopedia of volcanoes. Academic Press, San Diego, pp. 431–445

Patel A, Manga M, Carey RJ, Degruyter W (2013) Effects of thermal quenching on mechanical properties of pyroclasts. J Volcanol Geotherm Res 258:24–30

Polacci M, Burton MR, La Spina A, Murè F, Favretto S, Zanini F (2009) The role of syn-eruptive vesiculation on explosive basaltic activity at Mt. Etna, Italy. J Volcanol Geotherm Res 179(3):265–269

Reynolds P, Brown RJ, Thordarson T, Llewellin EW, Fielding K (2015) Rootless cone eruption processes informed by dissected tephra deposits and conduits. Bull Volcanol 77(9):1–17

Robert B, Harris A, Gurioli L, Médard E, Sehlke A, Whittington A (2014) Textural and rheological evolution of basalt flowing down a lava channel. Bull Volcanol 76(6):1–21

Sinton J, Grönvold K, Sæmundsson K (2005) Postglacial eruptive history of the western volcanic zone, Iceland. Geochem Geophys Geosyst 6(12)

Stovall WK, Houghton B, Gonnermann H, Fagents S, Swanson D (2011) Eruption dynamics of Hawaiian-style fountains: the case study of episode 1 of the Kīlauea Iki 1959 eruption. Bull Volcanol 73(5):511–529

Stovall WK, Houghton BF, Hammer JE, Fagents SA, Swanson DA (2012) Vesiculation of high fountaining Hawaiian eruptions: episodes 15 and 16 of 1959 Kīlauea Iki. Bull Volcanol 74(2):441–455

Thorarinsson S (1951) Laxárgljúfur and Laxárhraun: a tephrochronological study. Geogr Ann 33:1–89

Thorarinsson S (1953) The crater groups in Iceland. Bull Volcanol 14(1): 3–44

Thordarson T, Höskuldsson A (2002) Classic geology in Europe 3. Terra Publishing, Harpenden

von Komorowicz M (1912) Vulkanologische studien auf einigen inseln des Atlantischen Oceans. E. Schweizerbart, Stuttgart

Walker G, Croasdale R (1971) Characteristics of some basaltic pyroclastics. Bull Volcanol 35(2):303–317

Wilmoth RA, Walker GP (1993) P-type and S-type pahoehoe: a study of vesicle distribution patterns in Hawaiian lava flows. J Volcanol Geotherm Res 55(1):129–142

Wohletz K, McQueen R (1981) Experimental hydromagmatic volcanism. Amer Geophys.Union trans Eos 62(45):1085

Wohletz K, McQueen R (1984) Volcanic and stratospheric dustlike particles produced by experimental water-melt interactions. Geology 12(10):591–594

Wohletz KH (1983) Mechanisms of hydrovolcanic pyroclast formation: grain-size, scanning electron microscopy, and experimental studies. J Volcanol Geotherm Res 17(1–4):31–63

Wohletz KH (1986) Explosive magma-water interactions: thermodynamics, explosion mechanisms, and field studies. Bull Volcanol 48(5):245–264

Wohletz KH, Zimanowski B, Büttner R (2013) Magma-water interactions. In: Fagents SA, Gregg TKP, Lopes RMC (eds) Modeling volcanic processes. Cambridge University Press, New York, pp. 230–257

Zimanowski B (2001) Phreatomagmatic explosions. In: Freundt A, Rosi M (eds) From magma to tephra: modeling physical processes of explosive volcanic eruptions, developments in volcanology 4. Elsevier Science B.V, Amsterdam, pp. 25–54

Zimanowski B, Büttner R, Lorenz V, Häfele H-G (1997) Fragmentation of basaltic melt in the course of explosive volcanism. J Geophys Res: Solid Earth 102(B1):803–814

Zimanowski B, Wohletz K, Dellino P, Büttner R (2003) The volcanic ash problem. J Volcanol Geotherm Res 122(1):1–5